Kinetics-Informed Neural Representation for Dual-Tracer Dynamic PET Separation

Xingyue Wang[1†], Qing Ye[2†], Ganglin Liang[2], Yihuan Lu[2], and Zhiming Cui[1(✉)]

[1] School of Biomedical Engineering & State Key Laboratory of Advanced Medical Materials and Devices, ShanghaiTech University, Shanghai 201210, China
cuizm.neu.edu@gmail.com

[2] Shanghai United Imaging Healthcare Co., Ltd., Shanghai 201807, China

Abstract. Simultaneous dual-tracer positron emission tomography (PET) enables the acquisition of complementary physiological information within a single scan. However, separating individual tracer signals from mixed measurements remains a severely ill-posed inverse problem due to complex kinetic coupling and high noise levels in dynamic images. Traditional voxel-wise kinetic fitting suffers from heavy noise amplification and the need to estimate many kinetic parameters, while deep learning approaches rely on paired training data that are rarely available in clinical practice. In this work, we introduce a kinetics-informed neural representation framework for dual-tracer separation. Instead of estimating kinetic parameters independently for each voxel, we use a neural network that predicts tracer kinetic parameters from spatial coordinates. This shared representation introduces implicit spatial regularization, enabling spatially coupled and more robust parameter estimation. To realize this, the spatial coordinates are encoded using hash encoding and mapped to physiologically constrained kinetic parameters through an MLP. Then the predicted kinetic parameters are used in compartmental kinetic models to reconstruct separated dynamic images for each tracer. Experiments on both synthetic and real patient data demonstrate that the proposed method achieves superior separation performance compared with conventional and deep learning approaches, highlighting the potential of INR-based kinetic modeling for dual-tracer PET separation.

Keywords: Dynamic PET · Dual Tracer · Implicit Neural Representation · Kinetic Modeling

1 Introduction

Positron emission tomography (PET) is a molecular imaging modality that enables non-invasive quantification of physiological and biochemical processes in vivo [20]. It plays an important role in oncology, cardiology, and neurology using various radiotracers. For example, ^{18}F-fluorodeoxyglucose (FDG) reflects glucose metabolism and is widely used for tumor detection [22], while amino acid

† These authors contributed equally.

tracers such as ^{11}C-methionine (MET) provide complementary information for brain tumor characterization [2, 4]. Combining multiple tracers enables simultaneous assessment of complementary biological processes and improves characterization of disease heterogeneity. However, conventional dual-tracer imaging requires separate scans, increasing scan time, radiation exposure, and patient burden. Simultaneous dual-tracer PET addresses this limitation by acquiring mixed signals in a single scan, but separating tracer-specific activity remains fundamentally challenging [7]. Since all tracers emit indistinguishable 511 keV annihilation photons, signals from different tracers cannot be directly differentiated. Dual-tracer studies therefore employ dynamic acquisition with staggered injection to introduce temporal differences in tracer kinetics for signal separation. Early methods rely on compartmental kinetic modeling, where the measured signal is expressed as the sum of single tracer activities governed by individual kinetic parameters [3, 6]. These parameters are estimated from dynamic time activity curves (TACs) using graphical methods such as Patlak [19] and Logan plots [8], or nonlinear least-squares fitting such as Levenberg-Marquardt (LM) [9]. This kinetics-driven framework provides physiologically interpretable separation. However, voxel-wise LM fitting estimates parameters independently at each voxel, making it highly sensitive to noise and prone to spatially inconsistent parametric maps. Moreover, nonlinear fitting becomes less robust as the number of kinetic parameters increases, particularly in dual-tracer imaging where an irreversible two-tissue compartment (2TiC) model and a reversible two-tissue compartment (2TC) model are jointly estimated.

Recently, deep learning-based methods [5, 15, 21, 23, 26] have been proposed to predict single tracer images directly from mixed measurements. Although effective, these methods rely heavily on paired training data and primarily learn data-driven mappings without explicitly modeling tracer kinetics, limiting physiological interpretability and generalization to unseen protocols or tracer combinations. To address these issues, hybrid approaches [16, 17] have been proposed to incorporate kinetic modeling into deep learning frameworks. However, they still require synthetic data for supervised training, with restricted applicability in clinical settings where paired ground truth is unavailable. Implicit neural representation (INR) offers a promising alternative by modeling images as coordinate-based neural functions [10, 13, 18]. This formulation enables continuous spatial representation, compact modeling, and improved noise robustness. It has shown strong performance in medical imaging [11, 25], including PET reconstruction [12] and parametric imaging of single tracer [24]. By representing parametric maps as continuous functions, INR enables spatially coherent parameter estimation and improves spatial consistency compared with voxel-wise kinetic fitting.

Inspired by these advances, we propose a kinetics-informed implicit neural representation framework for dual-tracer PET separation. Specifically, we use a neural network to model tracer kinetic parameters as a continuous function of spatial coordinates, enabling spatially coupled parameter estimation across the entire image. Unlike existing deep learning methods, our approach directly

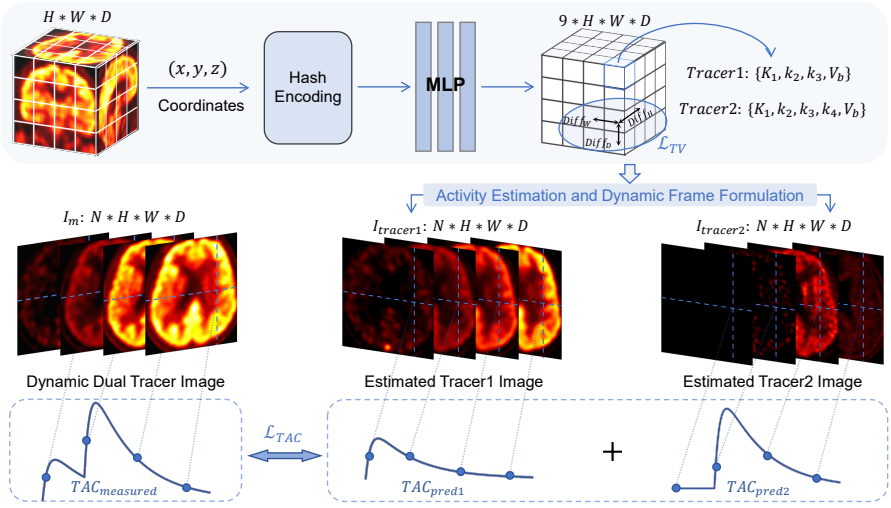

Fig. 1. Overview of our framework. Spatial coordinates are encoded using hash encoding and an MLP to estimate kinetic parameters, which are then used to obtain tracer TACs and compared to measured dual-tracer TACs.

estimates tracer kinetic parameters from measured dual-tracer dynamic images under explicit kinetic model constraints. The estimated kinetic parameters are then used to reconstruct activity of each tracer, ensuring physiologically consistent and efficient separation without requiring paired training data.

2 Method

Fig. 1 illustrates the overall pipeline of our proposed framework. Given dual-tracer dynamic PET images, our goal is to recover tracer-specific dynamics by estimating voxel-wise kinetic parameters. To this end, we model the kinetic parameters as a continuous neural field using instant-NGP [13], where spatial coordinates are encoded via multi resolution hash encoding and processed by a lightweight MLP to predict tracer specific parameters. Based on the estimated parameters, compartment models are used to establish the physiological relationship between tracer kinetics and tissue activity. An **Activity Estimation and Dynamic Frame Formulation** module obtains tracer concentrations using the analytical solution of the compartment model and integrates the resulting concentrations over acquisition frame durations to generate dynamic images for each tracer, denoted as I_{tracer1} and I_{tracer2}. During optimization, sampled voxel TACs from the estimated single tracer images are summed and compared with the measured dual-tracer TACs for model optimization. After optimization, the trained network can be queried at all spatial locations to obtain kinetic parameters and reconstruct dynamic images of each tracer, enabling accurate dual-tracer separation.

2.1 Activity Estimation and Dynamic Frame Formulation

Given the kinetic parameters of each voxel, tracer TACs can be analytically computed using compartmental modeling [1]. The TAC is given by the convolution of the plasma input function $C_p(t)$ with an impulse response defined by the kinetic parameters. For the irreversible two-tissue compartment model (2TiC), which is commonly used for tracers such as ^{18}F-FDG, the tissue concentration is given by:

$$C_{\text{Tracer1}}(t) = (1 - V_b)\left[K_1\left(\frac{k_3}{k_2 + k_3} + \frac{k_2}{k_2 + k_3}e^{-(k_2+k_3)t}\right) \otimes C_p(t)\right] + V_b C_B(t), \tag{1}$$

where K_1 ($\text{mL}\,\text{cm}^{-3}\,\text{min}^{-1}$), k_2 (min^{-1}), k_3 (min^{-1}), V_b and $C_B(t)$ denote the influx rate, efflux rate, phosphorylation rate, blood volume fraction, and the whole-blood activity concentration respectively. For the reversible two-tissue compartment model (2TC), which is commonly used for tracers such as ^{11}C-MET, the tissue concentration is computed as:

$$C_{\text{Tracer2}}(t) = (1 - V_b)\left[K_1\left(a_1 e^{-\alpha_1 t} + a_2 e^{-\alpha_2 t}\right) \otimes C_p(t)\right] + V_b C_B(t), \tag{2}$$

where a_1 and a_2 are coefficients of the exponential terms, α_1 and α_2 are the eigenvalues of the kinetic system determined by k_2, k_3, and k_4. Here, k_4 represents the dissociation rate constant with unit min^{-1}. The analytical expressions can be found in [1]. To match the actual PET acquisition process, the frame-wise activity is obtained by integrating the continuous TAC over each acquisition frame:

$$TAC_{\text{pred}} = \frac{1}{\Delta t_f}\int_{t_s}^{t_e} C_{\text{Tracer}}(t)dt, \tag{3}$$

where t_s and t_e denote the start and end times of frame f, and Δt_f is the frame duration. By applying this formulation to both tracers using their respective kinetic parameters, we obtain dynamic images I_{tracer1} and I_{tracer2}, from which the corresponding TACs are derived.

2.2 Model Optimization

The network is optimized using the total loss $\mathcal{L}$ defined as:

$$\mathcal{L} = \mathcal{L}_{TAC} + \mathcal{L}_{TV} + \mathcal{L}_{Vb}. \tag{4}$$

To ensure the predicted kinetic parameters accurately reconstruct the observed data, we minimize the Mean Squared Error (MSE) between the measured TAC ($TAC_{measured}$) and the sum of the predicted tissue compartments ($TAC_{pred1} + TAC_{pred2}$).

To suppress noise while preserving structural edges in the parametric maps, we implement a 3D total variation regularization. It is calculated as the sum of the mean squared differences between adjacent voxels along the depth, height, and width dimensions: $\mathcal{L}_{TV} = \text{Diff}_D + \text{Diff}_H + \text{Diff}_W$. In addition, to keep the fractional blood volume V_b within a biologically plausible range of $[0, 1]$, we introduce a constraint loss $\mathcal{L}_{V_b}$ that penalizes values outside this interval.

Table 1. Estimated FDG parameters of ROI (on synthetic data). WM: white matter, GM: gray matter.

	K1	k2	k3	Vb
	GT/Ours	GT/Ours	GT/Ours	GT/Ours
WM	0.0458/0.0469	0.1006/0.1242	0.0484/0.0302	0.0272/0.0272
GM	0.0970/0.0982	0.1311/0.1349	0.1693/0.0587	0.0997/0.0973

Table 2. Estimated MET parameters of ROI (on synthetic data). WM: white matter, GM: gray matter.

	K1	k2	k3	k4	Vb
	GT/Ours	GT/Ours	GT/Ours	GT/Ours	GT/Ours
WM	0.0383/0.0451	0.0636/0.2271	0.0361/0.1317	0.0286/0.1692	0.0265/0.0256
GM	0.0869/0.1051	0.0756/0.2858	0.1017/0.1906	0.0171/0.1086	0.1113/0.1206

3 Experiments and Results

We evaluated the proposed method on both synthetic data and real patient data. Our network is implemented using hash encoding with the parameters being set as $L = 16$, $T = 2^{17}$, $F = 4$, $N_{\min} = 8$, and $b = 2$. It is optimized using Adam with a learning rate of 1×10^{-3} and converged after 10,000 iterations. We compared our method with the traditional Levenberg-Marquardt (LM) algorithm [9] and a deep learning approach, DTS-INN [23]. Since DTS-INN requires paired 2D slices for training, we conducted experiments on the same synthetic 2D slices for comparison. Specifically, for synthetic data, both our method and DTS-INN were trained and evaluated on 2D slices. For real data, DTS-INN was applied slice by slice, and its 2D outputs were combined into 3D volumes for comparison with our 3D results.

3.1 Dataset Construction

Synthetic data To synthesize ^{18}F-FDG+^{11}C-MET dynamic PET images with ground truth, we performed Monte Carlo simulations on 12 digital brain phantoms generated from segmentations of clinical studies. Noise-free TACs for gray and white matter were generated by combining clinical input functions with kinetic parameters obtained from the literature [16] (i.e., K_1, k_2, k_3, V_b for FDG, and K_1, k_2, k_3, k_4, V_b for MET). A 65-min dual-tracer protocol was simulated by delaying the MET input function by 5 min relative to the FDG injection. These TACs, which accounted for radioactive decay, were then sampled at a 1-second resolution to simulate dynamic list-mode PET data on uMI Panorama PET/CT system. Dynamic data were then rebinned into 34 frames (6×10s, 4×30s, 2×60s, 6×10s, 4×30s, 1×120s, and 11×300s) for image reconstruction.

Clinical Patient Data Dual-tracer dynamic PET images were generated from two separate clinical scans of the same subject to validate the proposed method.

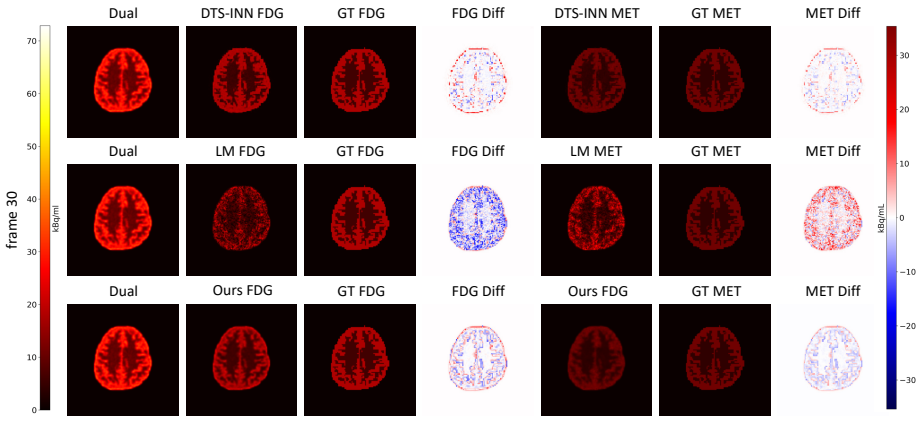

Fig. 2. Visual comparison of separated tracer images on synthetic data at frame 30.

The participant (female, 64 yrs, 44 kg) underwent 60-min PET acquisition on the uEXPLORER PET/CT system with 6.0 mCi ^{18}F-FDG administration at the bedside. A similar scan protocol was repeated on another day with injection of 10.0 mCi ^{18}F-AV45. With total-body coverage of uEXPLORER, image-derived input functions (IDIF) were extracted from descending aorta for each single tracer scan. For AV45, the whole blood-to-plasma and metabolite corrections were performed according to [14]. The brain regions were segmented from the two single tracer scans and subsequently co-registered via rigid registration. Dual-tracer PET images of 24×5s, 20×30s, and 48×60s were generated with AV45 injected 10 min after FDG injection.

3.2 Results of Synthetic Study

The estimated parameters for both tracers from a representative case are summarized in Table 1 and Table 2. Overall, our method produces parametric values within biologically plausible ranges compared with the ground truth (GT). However, noticeable deviations are observed for k_2 in white matter and k_3 in gray matter. These errors likely stem from the inherently ill-posed nature of the dual-tracer separation problem, which is further exacerbated by the increased number of kinetic parameters. As shown in Table 2, parameter estimation for the second tracer is more challenging due to its increased model complexity and higher number of unknown parameters. While some kinetic parameters exhibit biases, the reconstructed single tracer images remain visually comparable to the reference activity distributions, as shown in Fig. 2. Since the synthetic experiments directly simulated dual-tracer measurements to match real acquisition settings, paired single tracer measurements were not independently reconstructed. Therefore, the GTs shown in Fig. 2 correspond to activity templates generated from noise-free TACs in the simulation phantom, and the evaluation mainly relies on

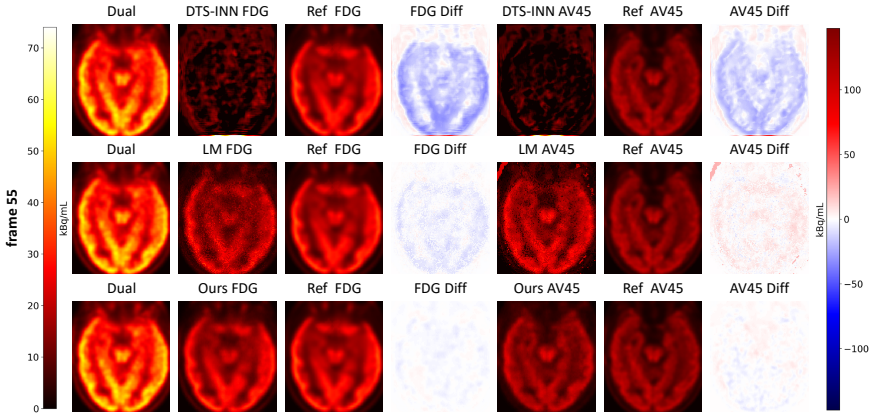

Fig. 3. Visual comparison of separated tracer images on real clinical data at frame 55.

visual comparison and TAC-based quantitative analysis. As illustrated, the proposed method achieves separation quality comparable to DTS-INN [23], despite not relying on supervised training with paired ground truth. In contrast, the traditional LM method [9] produces noticeably noisier results due to voxel-wise independent fitting.

To further assess temporal separation accuracy, we computed the NRMSE of ROI-level TACs across all synthetic cases (slice-level). Our method achieves 0.039 ± 0.024 for separated FDG, outperforming DTS-INN [23] (0.069 ± 0.054) and LM [9] (0.116 ± 0.030). For separated MET, our method obtains 0.049 ± 0.024, which is comparable to DTS-INN (0.047 ± 0.031) and substantially better than LM (0.172 ± 0.049). These results further indicate that our method better preserves the dynamic behavior of each tracer across frames.

3.3 Results on Clinical Patient Data

Fig. 3 presents the qualitative separation results for the 55th frame on real patient data. As shown in the figure, DTS-INN [23] exhibits noticeable performance degradation when applied to real scans. Since it is trained on paired synthetic data and treats temporal frames as separate input channels, its generalization is limited under different acquisition protocols. This limitation is reflected in the structural artifacts and the substantial discrepancies from the reference in the separated FDG and AV45 images. In comparison, the LM-based method [9] achieves improved tracer separation but still suffers from pronounced noise due to its voxel-wise independent fitting. In contrast, our proposed method produces better separation results with reduced noise and improved structural fidelity, showing the closest agreement with the reference.

The quantitative results in Table 3 further confirm these observations. On real patient data, metrics computed over nonzero dynamic frames show that our method consistently outperforms DTS-INN [23] and the LM-based method [9]

Table 3. Quantitative comparison on real patient data, with metrics computed on 3D volumes over nonzero dynamic frames.

Method	FDG			AV45		
	PSNR↑	SSIM↑	NRMSE↓	PSNR↑	SSIM↑	NRMSE↓
DTS-INN [23]	12.79±6.65	0.251±0.120	0.963±6.828	8.44±3.13	0.138±0.079	0.720±2.240
LM [9]	25.44±4.67	0.761±0.132	0.061±0.029	12.57±3.73	0.346±0.121	0.268±0.191
Ours	**31.75±3.25**	**0.935±0.024**	**0.027±0.008**	**23.40±1.69**	**0.766±0.074**	**0.069±0.012**

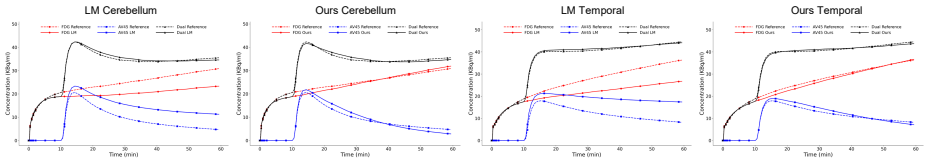

Fig. 4. Comparison of TACs in different ROIs between the proposed method and the traditional LM algorithm.

for both FDG and AV45 across PSNR, SSIM, and NRMSE. In particular, our method achieves substantially lower NRMSE while maintaining higher PSNR and SSIM, indicating more accurate tracer separation. These quantitative improvements are consistent with the visual results and demonstrate the practical advantage of our framework for real dual-tracer PET separation.

We further compared the TACs in the cerebellum and temporal cortex. As DTS-INN was trained on synthetic paired data and degraded heavily on real data, we focused the TAC comparison on our method and the traditional LM algorithm. Since TACs directly reflect tracer concentration changes over time, their agreement with the reference curves provides additional assessment of separation accuracy. As shown in Fig. 4, although the LM method produces a summed dual-tracer curve that closely matches the measured total activity, its estimated single-tracer TACs show substantial deviations from the reference curves. In contrast, our method achieves closer agreement with the reference TACs for both tracers. Despite minor residual differences, the improved curve alignment demonstrates the effectiveness of the proposed framework in recovering physiologically consistent tracer dynamics.

4 Conclusion and Discussion

In this work, we propose a kinetics-informed implicit neural representation framework for dual-tracer PET separation, which, to our knowledge, is the first INR-based solution for this task. By encoding 3D coordinates with hash encoding and estimating kinetic parameters under model constraints, our method enables spatially continuous and accurate tracer separation, improving robustness to noise compared with voxel-wise fitting. Unlike existing deep learning approaches, our

method does not require external paired training data and instead performs patient-specific optimization with improved practicality for clinical research.

Despite promising results, this study still has several limitations. For synthetic experiments, only dual-tracer measurements were simulated to match real acquisition settings, so the references shown in Fig. 2 are activity templates generated from noise-free TACs rather than independently acquired single tracer ground truths. This makes it difficult to perform rigorous image-level quantitative evaluation. In future work, we will consider simulating corresponding single tracer scans, similar to the evaluation setting used in the real study, so that the separated results can be assessed more comprehensively and quantitatively. In addition, extending the framework to more complex tracer combinations remains challenging due to increased ill-posedness, and clinical validation is limited by the scarcity of dual-tracer PET scans. Future studies will further validate the proposed method on such clinical data to support its application.

Acknowledgments. This work was supported by the National Natural Science Foundation of China (No. 6230012077), the Shanghai Municipal Central Guided Local Science and Technology Development Fund (No. YDZX20233100001001), the Beijing Natural Science Foundation (No. L242133), and the Capital's Funds for Health Improvement and Research (No. CFH2024-1-4101). We also acknowledge the support from the HPC Platform of ShanghaiTech University.

Disclosure of Interests. All authors declare no conflicts of interest.

References

1. Carson, R.E.: Tracer kinetic modeling in pet. In: Positron emission tomography: basic sciences, pp. 127–159. Springer (2005)
2. Galldiks, N., Law, I., Pope, W.B., Arbizu, J., Langen, K.J.: The use of amino acid pet and conventional mri for monitoring of brain tumor therapy. NeuroImage: Clinical **13**, 386–394 (2017)
3. Gao, F., Liu, H., Jian, Y., Shi, P.: Dynamic dual-tracer pet reconstruction. In: International Conference on Information Processing in Medical Imaging. pp. 38–49. Springer (2009)
4. Glaudemans, A.W., Enting, R.H., Heesters, M.A., Dierckx, R.A., van Rheenen, R.W., Walenkamp, A.M., Slart, R.H.: Value of 11c-methionine pet in imaging brain tumours and metastases. European journal of nuclear medicine and molecular imaging **40**(4), 615–635 (2013)
5. Huang, B., Xu, F., Shi, X., Huang, S., Li, B., Li, F., Liu, Q.: Pet tracer separation using conditional diffusion transformer with multi-latent space learning. arXiv preprint arXiv:2506.16934 (2025)
6. Kadrmas, D.J., Hoffman, J.M.: Methodology for quantitative rapid multi-tracer pet tumor characterizations. Theranostics **3**(10), 757 (2013)
7. Kadrmas, D.J., Rust, T.C.: Feasibility of rapid multi-tracer pet tumor imaging. In: IEEE Symposium Conference Record Nuclear Science 2004. vol. 4, pp. 2664–2668. IEEE (2004)

8. Logan, J., Fowler, J.S., Volkow, N.D., Wolf, A.P., Dewey, S.L., Schlyer, D.J., MacGregor, R.R., Hitzemann, R., Bendriem, B., Gatley, S.J., et al.: Graphical analysis of reversible radioligand binding from time—activity measurements applied to [n-11c-methyl]-(-)-cocaine pet studies in human subjects. Journal of Cerebral Blood Flow & Metabolism **10**(5), 740–747 (1990)
9. Marquardt, D.W.: An algorithm for least-squares estimation of nonlinear parameters. Journal of the society for Industrial and Applied Mathematics **11**(2), 431–441 (1963)
10. Mildenhall, B., Srinivasan, P., Tancik, M., Barron, J., Ramamoorthi, R., Ng, R.: Nerf: Representing scenes as neural radiance fields for view synthesis. In: ECCV (2020)
11. Molaei, A., Aminimehr, A., Tavakoli, A., Kazerouni, A., Azad, B., Azad, R., Merhof, D.: Implicit neural representation in medical imaging: A comparative survey. In: Proceedings of the IEEE/CVF International Conference on Computer Vision. pp. 2381–2391 (2023)
12. Moussaoui, Y., Mateus, D., Taheri, N., Moussaoui, S., Carlier, T., Stute, S.: Implicit neural representations for end-to-end pet reconstruction. In: 2025 IEEE 22nd International Symposium on Biomedical Imaging (ISBI). pp. 1–5. IEEE (2025)
13. Müller, T., Evans, A., Schied, C., Keller, A.: Instant neural graphics primitives with a multiresolution hash encoding. ACM transactions on graphics (TOG) **41**(4), 1–15 (2022)
14. Ottoy, J., Verhaeghe, J., Niemantsverdriet, E., Wyffels, L., Somers, C., De Roeck, E., Struyfs, H., Soetewey, F., Deleye, S., Van den Bossche, T., et al.: Validation of the semiquantitative static suvr method for 18f-av45 pet by pharmacokinetic modeling with an arterial input function. Journal of Nuclear Medicine **58**(9), 1483–1489 (2017)
15. Pan, B., Marsden, P.K., Reader, A.J.: Dual-tracer pet image separation by deep learning: a simulation study. Applied Sciences **13**(7), 4089 (2023)
16. Pan, B., Marsden, P.K., Reader, A.J.: Kinetic model-informed deep learning for multiplexed pet image separation. EJNMMI physics **11**(1), 56 (2024)
17. Pan, B., Marsden, P.K., Reader, A.J.: Self-supervised parametric map estimation for multiplexed pet with a deep image prior. Physics in Medicine & Biology **70**(4), 045002 (2025)
18. Park, J.J., Florence, P., Straub, J., Newcombe, R., Lovegrove, S.: Deepsdf: Learning continuous signed distance functions for shape representation. In: Proceedings of the IEEE/CVF conference on computer vision and pattern recognition. pp. 165–174 (2019)
19. Patlak, C.S., Blasberg, R.G., Fenstermacher, J.D.: Graphical evaluation of blood-to-brain transfer constants from multiple-time uptake data. Journal of Cerebral Blood Flow & Metabolism **3**(1), 1–7 (1983)
20. Phelps, M.E.: Pet: molecular imaging and its biological applications. Springer (2000)
21. Qing, M., Wan, Y., Huang, W., Xu, Y., Liu, H.: Separation of dual-tracer pet signals using a deep stacking network. Nuclear Instruments and Methods in Physics Research Section A: Accelerators, Spectrometers, Detectors and Associated Equipment **1013**, 165681 (2021)
22. Rohren, E.M., Turkington, T.G., Coleman, R.E.: Clinical applications of pet in oncology. Radiology **231**(2), 305–332 (2004)
23. Sun, C., Huang, B., Sun, J., Ni, Y., Liu, H., Xia, Q., Liu, Q., Zhu, W.: Temporal image sequence separation in dual-tracer dynamic pet with an invertible network. IEEE Transactions on Radiation and Plasma Medical Sciences **8**(7), 774–787 (2024)

24. Tehlan, K., Wendler, T.: Physiological neural representation for personalised tracer kinetic parameter estimation from dynamic pet. In: International Conference on Medical Image Computing and Computer-Assisted Intervention. pp. 491–500. Springer (2025)
25. Yang, B., He, P., Liu, S., Zhou, L.: Neural radiance fields enabled continuous pet image modeling and high-resolution reconstruction (2024)
26. Zeng, F., Fang, J., Muhashi, A., Liu, H.: Direct reconstruction for simultaneous dual-tracer pet imaging based on multi-task learning. EJNMMI research **13**(1), 7 (2023)